Progress In Electromagnetics Research, Vol. 135, 627–639, 2013

TEMPORAL MODULATION OF LIGHT INTENSITY VIA 1D TIME-VARIANT PHOTONIC CRYSTAL STRUCTURE

Zehui Yong[1], Zefeng Chen[1, 2], Yihang Chen[1, 2], Chi Wah Leung[1], Helen Lai Wa Chan[1], Bo Li[1, 3], and Yu Wang[1, *]

[1]Department of Applied Physics and Materials Research Center, The Hong Kong Polytechnic University, Hong Kong SAR, China

[2]Laboratory of Quantum Information Technology, School of Physics and Telecommunication Engineering, South Normal University, Guangzhou 510006, China

[3]Division of Energy & Environment, Graduate School at Shenzhen, Tsinghua University, Shenzhen 518055, China

Abstract—In this work, we show that light intensity modulation can be realized in the system of one-dimensional time-variant photonic crystals. Different from conventional light modulators, the functioning of the proposed structure emphasizes on its spatial/temporal structures instead of inherent material properties. Additionally, our system can perform inherent light modulation without introducing external stimuli, thus avoiding direct contacts with electrodes (or other modulation sources), which would be preferable in certain environments. The influences of parameters such as light frequency, structure dimensions, and refractive index contrasts on the modulation performance of the time-variant photonic crystal were investigated by numerical simulations. The results provide a new strategy for light modulation, which may add functionalities in optical communication, integrated-optics or display technologies.

Received 22 November 2012, Accepted 28 December 2012, Scheduled 3 January 2013

* Corresponding author: Yu Wang (yu.wang@polyu.edu.hk).

1. INTRODUCTION

Optical modulators are devices that can load information onto carrier light waves, either by intensity, phase, or polarizations. Conventionally, optical modulators are realized by taking advantages of inherent material properties, including 1) electro-optic effects in nonlinear optical materials ($LiNbO_3$ crystals or polymers) that are found in fiber optic processors [1–3]; 2) alignment of polarizations in liquid crystals, which are key components in display technologies [4, 5]; 3) electro-absorption effects in quantum wells, or silicon, which are generally applied in integrated optics [6–9]; 4) acousto-optic effects by refractive modulations in silica glasses using ultrasound waves [10, 11], and 5) magneto-optics [12, 13]. The modulating capabilities of these devices generally depend on external stimuli (e.g., applied voltages, ultrasound waves), which often need direct contacts with electrodes or vibrating crystals, thus limiting their applications in certain environments.

In recent decades, there is a rapid development of periodically structured dielectrics, also noted as photonic crystals (PC). In contrary to conventional optical materials, PCs emphasize on their microstructures rather than the material properties of individual components, which has led to peculiar properties such as optical band gaps, cavity resonance modes, and delicate manipulations of light passing through them. This strategy has also inspired a lot of applications, such as optical waveguide and microcavity lasers [14, 15]. However, realization of PC modulator is still limited — one approach is to tune the property of constituent material by electric or thermal means [16–18], which are essentially conventional modulators. Recently, we proposed a droplet-based time-variant photonic crystal (TvPC) [19] fabricated in microfluidic systems. The structure exhibits a "flowing" property and hence can introduce additional time-domain freedom of optical tuning.

In this paper, we show that optical modulation can be realized in transparent dielectrics without changing their material properties, by applying simultaneous spatial and temporal periodicity in a TvPC system. Additionally, with the aid of microfluidic system, TvPC modulators can act on their own without introducing external stimuli. The relationships between the modulation performance and the parameters of TvPCs are also discussed.

2. PRINCIPLES AND MODELLING

One-dimensional photonic crystals are generally constituted by alternatively layered structure [20–26], with refractive indices (RI) n_0

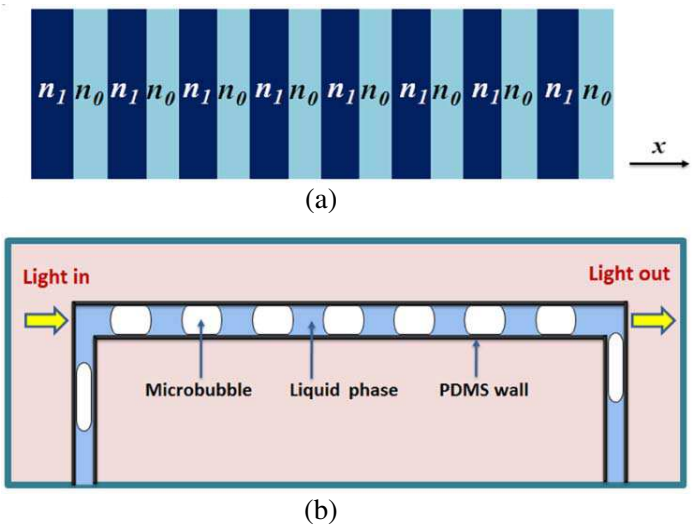

Figure 1. Schematic diagram of a TvPC. (a) 1D model of TvPC in layered structure; (b) a proposed microfluidic implementation of droplet-based TvPC in a U-shaped bend.

and n_1, as illustrated in Fig. 1(a). Our approach to form TvPC (i.e., to impose time-variant properties on conventional PCs) is to induce the movement of such a RI modulation along the x-axis. Fig. 1(b) shows one possible implementation of TvPC, which is constituted by periodic arrangements of microbubbles and liquid phases in a U-shaped bend cladded by thin transparent walls (e.g., PDMS). Such a structure can be realized in microfluidic system, using microdroplet formation techniques such as flow-focusing or T-junction methods — the droplets thus formed are inherently periodic and monodispersed — as discussed in Ref. [19]. However, in consideration of calculation costs, we resorted to the more general and idealized 1D layered structure (Fig. 1(a)). The non-critical details of the considered system (such as bubble sizes, shapes, wall thickness, etc.) were ignored while all important modulation features were retained.

Transfer scattering matrix method (TSMM) can be used to investigate the optic transmissions of TvPC along the x-axis. For the model in Fig. 1(a), the total power transmittance can be written as

$$I = \left|S_{11} - S_{12}S_{21}/S_{22}\right|^2, \tag{1}$$

where S is the total scattering matrix of the layered structure, which

is defined as

$$S = \overbrace{M_{ij}P_jM_{ji}P_i}^{MPMP}\overbrace{\cdots\cdots\cdots\cdots}^{(MPMP)^{N-2}}M_{ij}P_jM_{ji} = \begin{pmatrix} S_{11} & S_{12} \\ S_{21} & S_{22} \end{pmatrix}, \quad (2)$$

where S_{11}, S_{12}, S_{21}, S_{22} are elements of scattering matrix S, and N is the number of periods in a 1D finite periodic structure, M_{ij} the scattering matrix describing interface reflection/transmission between two different layers with RIs n_i and n_j, respectively, and P_i the propagation matrix corresponding to layer i. The two matrices can be expressed as

$$M_{ij} = \frac{1}{2}\begin{pmatrix} 1 + n_i/n_j & 1 - n_i/n_j \\ 1 - n_i/n_j & 1 + n_i/n_j \end{pmatrix} \quad (3)$$

and

$$P_i = \begin{pmatrix} \exp(-in_i\omega d_i/c) & 0 \\ 0 & \exp(in_i\omega d_i/c) \end{pmatrix}, \quad (4)$$

where d_i is the thickness of the corresponding layer i. In the model of Fig. 1(a), $N = 8$, $n_i = n_0$, and $n_j = n_1$.

3. RESULTS AND DISCUSSIONS

3.1. Frequency Responses and Time Responses in TvPC

Because of the dynamic nature, the RI distribution in the TvPC is a function of spatial coordinate x and time t such that $n(x, t) = n(x - R, t - T)$, where R is the spatial periodicity, and $T = R/v$ is the time period for a TvPC to restore its configuration as the structure moves, with v being the speed of RI modulation movement. We first study the optical properties of TvPC at 4 different time frames: $t = 0$, $t = T/4$, $t = T/2$, and $t = 3T/4$, as shown in Fig. 2(a). In this model, the two types of layers with higher RI n_1 and lower RI n_0 are of equal thickness. The total length of the TvPC is set to be $L = 3.3R$. The left and right parts are infused with air ($n_0 = 1$) to represent the free space. At $t = 0$, the order of layer arrangement is $(ABABABA_{0.3})$, where A and B represent the higher- and lower-RI layers with identical thickness of $0.5R$ unless stated otherwise. For example, $A_{0.3}$ represents a higher-RI layer with the thickness of $0.3R$, as indicated in the subscript. Similarly, for $t = T/4$, $t = T/2$, and $t = 3T/4$, the layer structures are $(B_{0.25}ABABABA_{0.05})$, $(BABABAB_{0.3})$, $(A_{0.25}BABABAB_{0.05})$, respectively.

Figure 2(b) shows four transmittance spectra corresponding to the TvPC configurations presented in Fig. 2(a), with RIs $n_1 = 1.4$ and $n_0 = 1.0$ ($n_1 = 1.4$ is an average RI of common fluids, e.g., water,

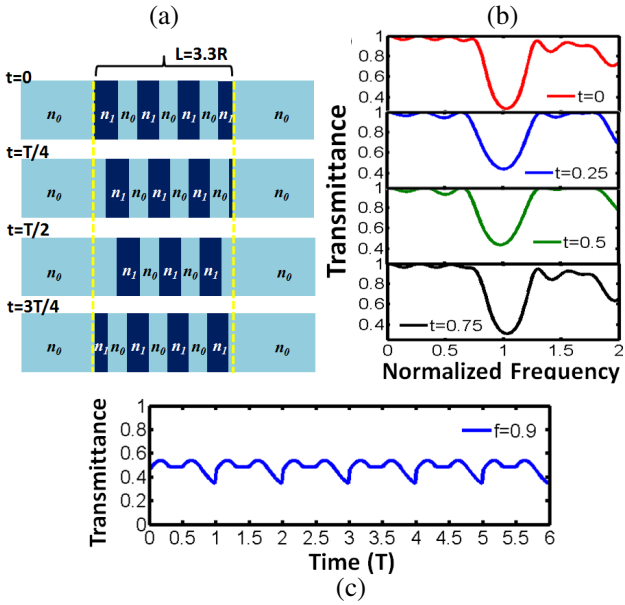

Figure 2. Frequency and time responses of TvPC: (a) model of TvPC for $t = 0$, $T/4$, $T/2$ and $3T/4$; (b) transmittance of TvPC for $t = 0$, $T/4$, $T/2$ and $3T/4$ at $f = 0$ to 2; (c) transmittance of TvPC at $f = 0.9$ for $t = 0$ to $6T$. Simulation configuration for (b) and (c) are, $n_0 = 1$ and $n_1 = 1.4$.

carbon tetrachloride, benzene, etc.). Frequency is normalized by the unit $c/[(n_0+n_1)R]$. The transmittances changes slightly as the periodic structure moves. The ripples in the spectra were caused by grating effects. An example of the modulation is shown in Fig. 2(c), where the variations of transmittance corresponding to normalized frequency $f = 0.9$ in the period of time $0 \sim 6T$ are shown and a complex waveform is presented.

An important figure of merit in intensity modulation is the optical modulation index ΔI, which is defined as modulation of output power divided by the input power, or equal to the difference of transmittance $I_{\max}$-$I_{\min}$; in Fig. 2(c) this is equal to 0.27. The performance of an intensity modulator mainly depends on the value of ΔI that will be discussed in details in next sections.

3.2. Light Modulation in TvPCs with Different Lengths

To further study the modulation properties of TvPCs, we introduce a diagram named "modulation spectra", which can simultaneously

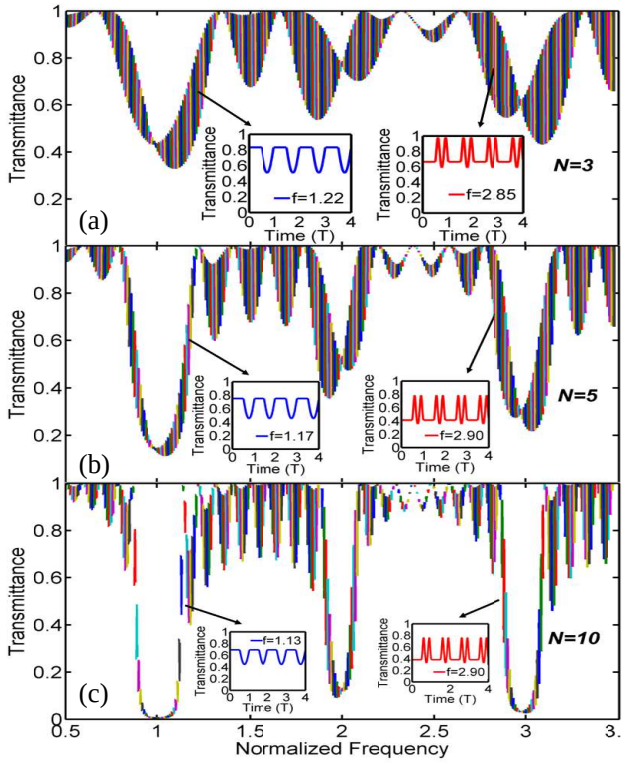

Figure 3. Modulation spectra of TvPC with RI contrast $n_1 : n_0 = 1.4$ for (a) 3 periods, (b) 5 periods and (c) 10 periods. Vertical bars at each frequency show the maximum and minimum of modulation amplitude. Insets show modulation waveforms at particular frequencies.

display the frequency responses and modulation properties, as shown in Fig. 3. In the modulation spectra, conventional transmittance spectra — which show basic features such as bandgaps and grating ripples — are overlapped by colored vertical bars. These bars represent the intensity modulation index ΔI, at particular frequency points, with their lower ends indicating the lowest transmittance level $I_{\min}$, and upper ends indicating the highest transmittance level $I_{\max}$. Insets in Fig. 3 show detailed modulation waveforms at particular frequency points. The three different modulation spectra are TSMM results of three finite TvPC structures, with the same RI contrast $n_1/n_0 = 1.4$, different number of layer repeats ($N = 3$ (Fig. 3(a)), $N = 5$ (Fig. 3(b)) and $N = 10$ (Fig. 3(c)), respectively). The studied normalized frequencies range from 0.5 to 3.5. In Fig. 3 there are several interesting properties as stated below:

First, the basic features of finite photonic crystals are clearly shown: when the number N gets larger, the bandgaps become pronounced and the bandedges get steeper. One special bandgap is that centered at $f = 2.0$, which is very weak (undistinguishable from grating ripples) for $N = 3$, but gets fairly prominent at $N = 5$ and $N = 10$. For grating ripples, there are no obvious variations of their depths; however the number of grating ripples gets larger, as N increases (equal to N-2).

Secondly, the modulation amplitudes ΔI, i.e., the lengths of vertical bars, varies as the frequency changes in each configuration. From the figures, we can see ΔI gets its largest value at bandedge areas and grating ripples. Time responses for bandedge modulations near the 1st and the 3rd bandgaps are shown in insets.

Thirdly, the dispersion effect, i.e., the instability of transmittance with respect to frequency, gets stronger when N increases (shown by the slopes indicated by arrows). These effects would limit the bandwidth performance of TvPC as an optical intensity modulator. Therefore, in further studies only structures with smaller N were considered.

In practice, integral number of periods cannot be accurately defined on the length of U-shaped bend (the structure shown in Fig. 1(a)); thus it is interesting to study fractional periods, as shown in Fig. 4(a) (for $N = 3.2$) and Fig. 4(b) (for $N = 3.8$). A prominent feature in Fig. 4 is that, the modulation indices ΔI, represented by colored vertical bars, become symmetrical, opposite to the highly asymmetric bars shown in Fig. 3. Meantime, the heaviest modulations shift from bandedge frequencies to the centers of bandgaps. For $N = 3.2$, the three bandgaps all show large ΔI, for example at $f = 1.0$ ($\Delta I = 0.4$) and $f = 2.0$ ($\Delta I = 0.34$); while for $N = 3.8$, ΔI in 1st bandgap weakens, but gets stronger at the 2nd and the 3rd bandgap, as shown in the insets ($\Delta I = 0.41$ at $f = 2.0$, and $\Delta I = 0.35$ at $f = 3.0$).

Now we introduce a 2D diagram named "modulation map", which demonstrates the dependence of ΔI on the normalized frequency and period number N as a color map. Fig. 5 shows such a modulation map, for TvPCs with the same RI contrasts as those in Fig. 4. Values for ΔI span from 0 (blue) to 0.47 (red). The most obvious feature in Fig. 5 is the distribution of patches with high ΔI (which we term as "high ΔI islands"). These "islands" can be categorized as "bandedge modulation islands", "gap center modulation islands", and "grating ripple modulation islands", according to the frequencies at which they occur. Another feature is the abrupt changes, located at integral period numbers N, where ΔI is discontinuous.

Generally, for period numbers $3 < N < 3.6$ and $4 < N < 4.6$, ΔI

remains weak and shows no variations as a function of N. Obvious variations occur when $3.6 < N < 4$ and $4.6 < N < 5$. For the 1st bandgap (around $f = 1$), there are no gap center modulations; the left and right "bandedge islands" appear and blue-shift slightly as N

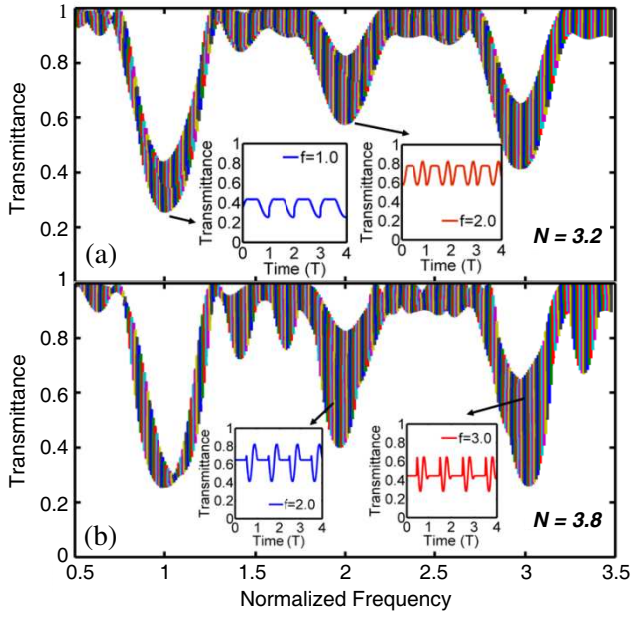

Figure 4. Modulation spectra of TvPC with RI contrast $n_1 : n_0 = 1.4$ for (a) 3.2 periods and (b) 3.8 periods.

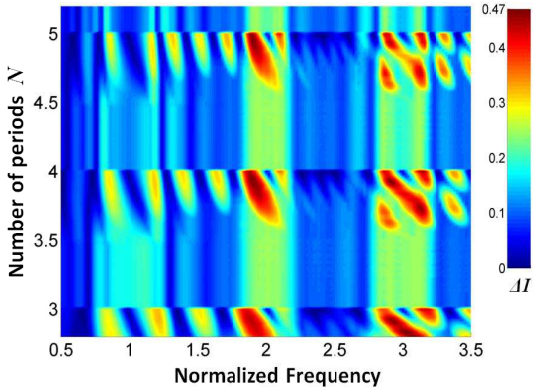

Figure 5. Modulation map of TvPC (ΔI vs. frequency and period number N) with RI contrast $n_1 : n_0 = 1.4$.

increases. For the 2nd bandgap, modulations occur first at the gap center and gradually blue-shift to bandedges; for N close to integral values small right "bandage islands" appear. For the 3rd bandgap, the "high ΔI islands" are split into four parts, and gap center modulations only occur near $N = 3.8$ or 4.8. For frequencies between bandgaps, the islands demonstrate ripple modulations due to grating-like effect, which are also blue-shifted as N increases. These heavy modulations are actually due to structure of photonic crystals — normal gratings (where the spatial period R is much smaller than wavelength) cannot cause large modulations, such as that at $f = 0.6$. These modulations can also be very large, for example between 3rd and 4th bandgaps; but sometimes they do not even show up at all, for example between 2nd and 3rd bandgaps. At last, all these islands "bandedge", "gap center" and "grating ripple" suddenly disappear at integral values of N, above which the features are essentially repeated.

Modulation maps for TvPC with other RI contrasts were also calculated (not shown here). Gap center modulations were only present at low RI contrast TvPCs. For large RI contrasts, bandgaps were too pronounced which prohibited the observation of any gap center modulations; bandedge/grating modulations were the main observations. The dependence of ΔI on RI contrasts are discussed in the next section.

3.3. Light Modulation in TvPCs with Different RI Contrast

RI indices of the constituent materials have significant impact on the electromagnetic properties of TvPCs. As in conventional photonic crystals, higher RI contrast could lead to deeper and wider bandgaps. Fig. 6 shows the modulation spectra for TvPCs with the same period number $N = 3.8$ as that in Fig. 5(b), while the RI contrasts n_1/n_0 is 1.6 (Fig. 6(a)) and 1.8 (Fig. 6(b)), respectively. Compared with Fig. 5(b), all three bandgaps become deeper and wider. As for ΔI, the ability for modulation diminishes as the contrast of the 2nd bandgap increases, but for the 3rd bandgap ΔI increases a lot. The heaviest modulation can be found at $f = 3.10$ in inset of Fig. 6(b).

Detailed dependence of ΔI on RI contrast for TvPCs with $N = 3.8$ is presented in the modulation map, as shown in Fig. 7. Several characteristics can be observed from this figure. First, no obvious modulation occurs when the RI contrast is very small since TvPC acts like a homogeneous medium in this region. When the value of RI contrast becomes larger, obvious grating ripple modulations and bandedge modulations can be found in various frequencies in the TvPC. However, the changes of ΔI are quite different in the three bandgaps. For the 1st bandgap, only bandedge modulations can be

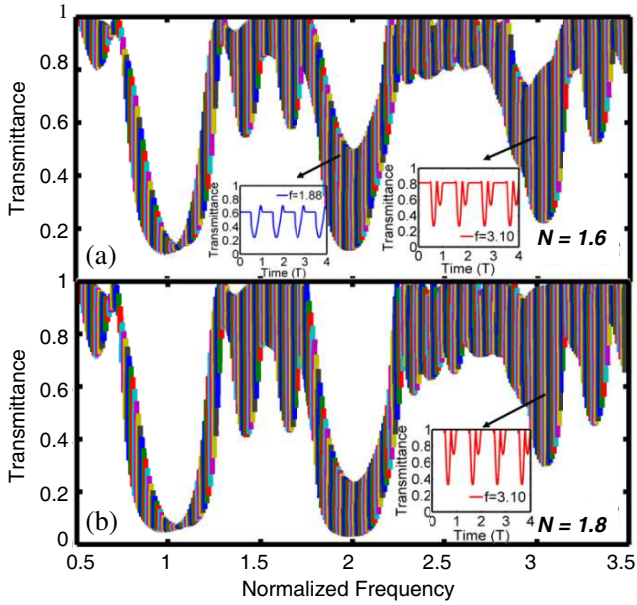

Figure 6. Modulation spectra of TvPC with period number $N = 3.8$ and RI contrast (a) $n_1 : n_0 = 1.6$ and (b) $n_1 : n_0 = 1.8$.

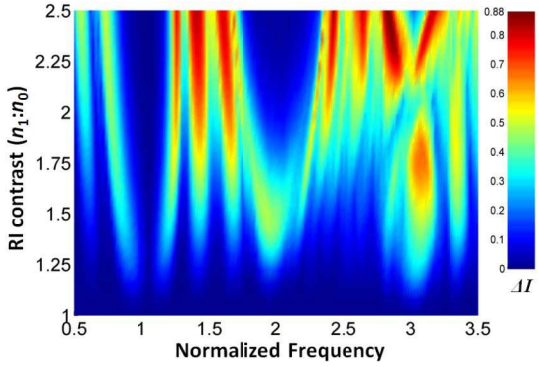

Figure 7. Modulation map of TvPC (ΔI vs. frequency and RI contrasts $n_1 : n_0$) with period number $N = 3.8$.

seen, the gap center modulation is suppressed since the bandgap is too deep to allow any transmission of light within the gap. For the 2nd bandgap, gap center modulation exists at $n_1/n_0 = 1.3 \sim 1.6$ since the bandgap is actually shallow. As the RI contrast increases to a relatively large value ($n_1/n_0 > 1.6$), the gap becomes deeper and

the gap center modulation disappears. For the 3rd bandgap, stronger gap center modulation can be observed. Such gap center modulation discontinues at $n_1/n_0 = 2$ since the 3rd bandgap disappears.

4. CONCLUSION

In conclusion, light intensity modulation based on TvPC is proposed and demonstrated. Using the dynamic nature of the proposed system, the intensity and waveform of the transmitted light can be modulated without additional stimuli. Three kinds of modulations (with bandgap center, bandedges, and grating ripples, respectively) are observed in TvPCs, as evidenced in modulation spectra and modulation map, by TSMM calculations. The relationships between these modulations and various parameters are also investigated; proper selection of structure dimensions and refractive indices are critical for efficient TvPC designs. We believe the proposed approach to light modulation may shed light in both photonic crystal and optofluidic studies.

ACKNOWLEDGMENT

This work is supported by the Hong Kong ITF Project (K-ZS0B) and the Hong Kong Polytechnic University (1-ZV8T, J-BB9P).

REFERENCES

1. Gopalakrishnan, G. K., W. K. Burns, R. W. McElhanon, C. H. Bulmer, and A. S. Greenblatt, "Performance and modeling of broadband $LiNbO_3$ traveling wave optical intensity modulators," *J. Lightwave Technol.*, Vol. 12, 1807–1819, 1994.
2. Shi, Y., C. Zhang, H. Zhang, J. H. Bechtel, L. R. Dalton, B. H. Robinson, and W. H. Steier, "Low (sub-1-volt) halfwave voltage polymeric electro-optic modulators achieved by controlling chromophore shape," *Science*, Vol. 288, 119–122, 2000.
3. Enami, Y., C. T. Derose, D. Mathine, C. Loychik, C. Greenlee, R. A. Norwood, T. D. Kim, J. Luo, Y. Tian, A. K.-Y. Jen, and N. Peyghambarian, "Hybrid polymersol-gel waveguide modulators with exceptionally large electro-optic coefficients," *Nat. Photon.*, Vol. 1, 180–185, 2007.
4. Lu, K. and B. E. A. Saleh, "Theory and design of the liquid crystal TV as an optical spatial phase modulator," *Opt. Eng.*, Vol. 29, 240–246, 1990.

5. Weiner, A. M., D. E. Leaird, J. S. Patel, and J. R. Wullert, "Programmable shaping of femtosecond optical pulses by use of 128-element liquid crystal phase modulator," *IEEE J. Quantum Electron.*, Vol. 28, 908–920, 1992.
6. Zucker, J. E., K. L. Jones, B. I. Miller, and U. Koren, "Miniature Mach-Zehnder InGaAsP quantum well waveguide interferometers for 1.3 μm," *IEEE Photon. Technol. Lett.*, Vol. 2, 32–34, 1990.
7. Fetterman, M., C.-P. Chao, and S. R. Forrest, "Fabrication and analysis of high-contrast InGaAsP-InP Mach-Zehnder modulators for use at 1.55-μm wavelength," *IEEE Photon. Technol. Lett.*, Vol. 8, 69–71, 1996.
8. Liu, A., R. Jones, L. Liao, D. Samara-Rubio, D. Rubin, O. Cohen, R. Nicolaescu, and M. Paniccia, "A high-speed silicon optical modulator based on a metal-oxide-semiconductor capacitor," *Nature*, Vol. 427, 615–618, 2004.
9. Xu, Q., B. Schimidt, S. Pradhan, and M. Lipson, "Micrometre-scale silicon electro-optic modulator," *Nature*, Vol. 435, 325–327, 2005.
10. Rhodes, W. T., "Acousto-optic signal processing: Convolution and correlation," *Proc. IEEE*, Vol. 69, 65–79, 1981.
11. Dugan, M. A., J. X. Tull, and W. S. Warren, "High-resolution acousto-optic shaping of unamplified and amplified femtosecond laser pulses," *J. Opt. Soc. Am. B*, Vol. 14, 2348–2358, 1997.
12. Ross, W. E., D. Psaltis, and R. H. Anderson, "Two-dimensional magneto-optic spatial light modulator for signal processing," *Opt. Eng.*, Vol. 22, 485–490, 1983.
13. Davis, J. A., E. Carcole, and D. M. Cottrell, "Intensity and phase measurements of nondiffracting beams generated with a magneto-optic spatial light modulator," *Appl. Opt.*, Vol. 35, 593–598, 1996.
14. Lin, S.-Y., E. Chow, V. Hietala, P. R. Villeneuve, and J. D. Joannopoulos, "Experimental demonstration of guiding and bending of electromagnetic waves in a photonic crystal," *Science*, Vol. 282, 274–276, 1998.
15. Painter, O., R. K. Lee, A. Scherer, A. Yariv, J. D. O'Brien, P. D. Dapkus, and I. Kim, "Two-dimensional photonic band-gap defect mode laser," *Science*, Vol. 284, 1819–1821, 1999.
16. Jim, K. L., D. Y. Wang, C. W. Leung, C. L. Choy, and H. L. W. Chan, "One-dimensional tunable ferroelectric photonic crystals based on $Ba_{0.7}Sr_{0.3}TiO_3$/MgO multilayer thin films," *J. Appl. Phys.*, Vol. 103, 083107, 2008.
17. Zhou, J., C. Q. Sun, K. Pita, Y. L. Lam, Y. Zhou, S. L. Ng,

C. H. Kam, L. T. Li, and Z. L. Gui, "Thermally tuning of the photonic band gap of SiO_2 colloid-crystal infilled with ferroelectric $BaTiO_3$," *Appl. Phys. Lett.*, Vol. 78, 661–663, 2001.

18. Li, B., J. Zhou, L. Li, X. J. Wang, X. H. Liu, and J. Zi, "Ferroelectric inverse opals with electrically tunable photonic band gap," *Appl. Phys. Lett.*, Vol. 83, 4704–4706, 2003.
19. Chen, Z., Z. Yong, C. W. Leung, X. Zhang, Y. Chen, H. L. W. Chan, and Y. Wang, "Time-variant 1D photonic crystals using flowing microdroplets," *Opt. Express*, Vol. 20, 24330–24341, 2012.
20. Srivastava, S. K. and S. P. Ojiha, "Enhancement of omnidirectional reflection bands in one-dimensional photonic crystals with left-handed materials," *Progress In Electromagnetics Research*, Vol. 68, 91–111, 2007.
21. Srivastava, S. K. and S. P. Ojiha, "Photonic band gaps in one-dimensional metallic star waveguide structure," *Progress In Electromagnetics Research*, Vol. 84, 349–362, 2008
22. Banerjee, A., "Enhanced refractometric optical sensing by using one-dimensional ternary photonic crystals," *Progress In Electromagnetics Research*, Vol. 89, 11–22, 2009.
23. Wu, C.-J., Y.-H. Chung, B.-J. Syu, and T.-J. Yang, "Band gap extension in a one-dimensional ternary metal-dielectric photonic crystal," *Progress In Electromagnetics Research*, Vol. 102, 81–93, 2010.
24. Dai, X., Y. Xiang, and S. Wen, "Broad omnidirectional reflector in the one-dimensional ternary photonic crystals containing superconductor," *Progress In Electromagnetics Research*, Vol. 120, 17–34, 2011.
25. Tolmachev, V. A., A. V. Baldycheva, K. Berwick, and T. S. Perova, "Influence of fluctuations of the geometrical parameters on photonic band gaps in one-dimensional photonic crystals," *Progress In Electromagnetics Research*, Vol. 126, 285–302, 2012.
26. Wu C.-J., T.-J. Yang, C.-C. Li, and P.-Y. Wu, "Investigation of effective plasma frequencies in one-dimensional plasma photonic crystals," *Progress In Electromagnetics Research*, Vol. 126, 521–538, 2012.